INORGANIC CHEMISTRY FRONTIERS

RESEARCH ARTICLE

View Article Online
View Journal | View Issue

Cite this: *Inorg. Chem. Front.*, 2023, **10**, 7351

Multi-stimulus responsive properties of a Cd-MOF based on tetraphenylethylene†

Chen Wang,[a] Ting Zhang,[a] Li-Xian Sun,[b] Yong-Heng Xing *[a] and Feng-Ying Bai *[a]

Received 25th September 2023,
Accepted 3rd November 2023

DOI: 10.1039/d3qi01954c

rsc.li/frontiers-inorganic

Multi-stimulus-responsive materials possess potential practical application capabilities in anti-counterfeiting, sensing, information storage and other fields. Here, we have synthesized a crystalline material, **Cd-tcbpe** MOF, based on a TPE derivative by a "two-step" method with a high yield. This crystalline MOF material exhibits sensitive and reversible fluorescence color changes from cyan to yellow–green in response to multiple stimuli including mechanical forces, water, some small molecules (*i.e.* NH_3, CH_3COOH, CF_3COOH, and HCl vapors) and temperature. Notably, the corresponding ligand alone does not possess these multi-stimulus responsive properties. We found that the changes in fluorescence properties are benefited from the compression and extension of the ligand in the MOF framework structure. This work also provides support for the development of white LED materials, mechanical flaw detection materials and water vapor/temperature detection.

1. Introduction

Multi-stimulus-responsive materials, which can undergo changes in physical/chemical properties in response to more than two stimulus conditions, such as light, electricity, temperature and force,[1–3] have shown great potential in sensing and information storage.[4–7] Famous cases of organic small molecules such as azo-benzene,[8] spiropyran[9] and viologen[10] have been widely studied for multi-stimulus responsive materials, which could respond to multiple stimuli. However, their tedious synthesis conditions and aggregation-caused quenching (ACQ) in the solid state hinder their application especially in the fluorescence area.[11] In contrast to ACQ, aggregation-induced emission (AIE) first reported by Tang *et al.* in 2001,[12] due to the limitation of non-radiative transitions, resulting in strong fluorescence in both solid and thin films, was achieved. To date, molecules with AIE properties have attracted widespread attention from many researchers and have been applied in chemical sensing,[13,14] stimulus-responsive materials,[15] and other fields. As a molecule with a propeller structure, tetraphenylethylene (TPE) is a star molecule in the AIE field. However, TPE molecules only exhibit mechanochromic luminescence behavior and fluorescence properties.[16] Thus, to achieve responses to stimuli, the structural modification of TPE molecules is inevitable, which however requires complex synthesis and the use of expensive metal catalysts,[17] in some cases. In addition, some modified TPE molecules may even lose their mechanochromic luminescence behavior.[18] Therefore, obtaining TPE derivatives with multi-stimulus response properties remains a challenge.

Metal–organic frameworks (MOFs) are a fascinating class of inorganic–organic hybrid crystalline materials with high porosity, excellent surface areas and a tunable pore structure.[19–25] And they are regarded as a platform for sensing,[26] gas adsorption/separation,[27,28] catalysis,[29] and so on. It is worth noting that benefiting from the framework structure, some functionalized MOFs display certain properties that the corresponding ligands do not possess.[30] Therefore, MOFs based on TPE molecules might have the potential for the preparation of multi-stimulus responsive materials,[31] which are however seldom reported.[32]

Herein, starting from a TPE based ligand H_4tcbpe (4′, 4‴, 4⁗, 4⁗′-(ethene-1,1,2,2-tetrayl)tetrakis(([1,1′-bipheny]-4-carboxylic acid))), a three-dimensional porous network structure, **Cd-tcbpe**, was constructed with Cd^{2+} as the metal source. The crystalline **Cd-tcbpe** exhibits obvious luminescence changes from cyan to yellow–green under the stimulations of mechanical forces, water, volatile acid/base small molecules and temperature. Nevertheless, this phenomenon cannot be found in the ligand H_4tcbpe. Benefiting from such multi-stimulus-respon-

[a]*College of Chemistry and Chemical Engineering, Liaoning Normal University, Huanghe Road 850#, Dalian, 116029, P. R. China.*
E-mail: xingyongheng2000@163.com, baifengying2003@163.com
[b]*Guangxi Key Laboratory of Information Materials, Guilin University of Electronic Technology, Guilin 541004, P. R. China*

†Electronic supplementary information (ESI) available: Materials and methods, X-ray crystallographic determination, structural description of **Cd-tcbpe**, fluorescence spectra, FT-IR spectra, PXRD patterns, and fluorescence lifetimes. CCDC 2284476. For ESI and crystallographic data in CIF or other electronic format see DOI: https://doi.org/10.1039/d3qi01954c

sive character, **Cd-tcbpe** has shown great potential for information storage, anti-counterfeiting, white LED lighting, luminescence sensing, *etc*.

2. Experimental section

2.1 Synthesis of $[Cd_3(tcbpe)_{1.5}(DMF)(H_2O)_2]\cdot 6DMF$ (Cd-tcbpe)

In a glass vial, 1 mL of DMF solvent was added to 8.1 mg (0.01 mmol) of H_4tcbpe ligand. The mixture was sonicated until the solid was totally dissolved to form a transparent yellow solution. Then 0.5 mL of ethanol was added, and the mixture was heated at 85 °C for 12 hours. Before cooling down to room temperature, 30.8 mg (0.1 mmol) of $Cd(NO_3)_2\cdot 4H_2O$ was added. The mixture was sonicated until the solid was totally dissolved, and then was transferred to an 85 °C oven for 12 h to afford yellow solutions and pale-yellow crystals of **Cd-tcbpe**. Anal. calcd (%) for $C_{102}H_{101}Cd_3O_{21}N_7$: C, 58.34; H, 4.81; N, 4.67. Found (%): C, 58.37; H, 4.78; N, 4.63. IR data (cm^{-1}): 3424, 3032, 2932, 1647, 1583, 1383, 1177, 1091, 835, 782.

2.2 Preparation of the Cd-tcbpe-B@PMMA film

The **Cd-tcbpe-B**@PMMA film adopts a three-layer sandwich structure. The upper and bottom layers are pure PMMA polymers to prevent the color change of **Cd-tcbpe** due to contact with air. The preparation process of the middle layer is as follows: PMMA (1.75 g) was added to CH_3CN (10 mL) and mixed at room temperature for 12 h. Then 1 mL of the above solution and 25 mg of **Cd-tcbpe-B** were fully mixed and applied to a glass slide, and dried in a glass dryer to finally form a **Cd-tcbpe-B**@PMMA film (Scheme S1†).

3. Results and discussion

3.1 Synthesis discussion

Generally, the TPE based MOFs reported are constructed by a traditional "one pot" method, in which all the reactants including the ligands, metal salts and solvents are added at one time during the solvothermal and hydrothermal reactions. However, here we adopted a modified "two-step" strategy to synthesize **Cd-tcbpe**, that is, thoroughly heating and dissolving the ligand before adding the metal salt, and subsequently heating. Such a synthetic method greatly improved the yield of MOFs by 1.17 times from the original 28.6% to 62.0% (Scheme 1). The detailed "one pot" method of synthesizing **Cd-tcbpe** is given in the ESI.† To figure out the differences in the apparent morphology, atomic force microscopy (AFM) testing was conducted to analyse the surface morphology of the solutions with and without preheating. As displayed in Fig. S1,† the grain height of the preheated ligand solution is much more uniform than that of the corresponding ligand solution without heating. Thus, it is suggested that the preheating procedure could help better disperse the ligand, which is beneficial for the coordination reaction between the ligand and the metal salt. We believe that our strategy might provide an alternative to improve the yields of some MOFs.

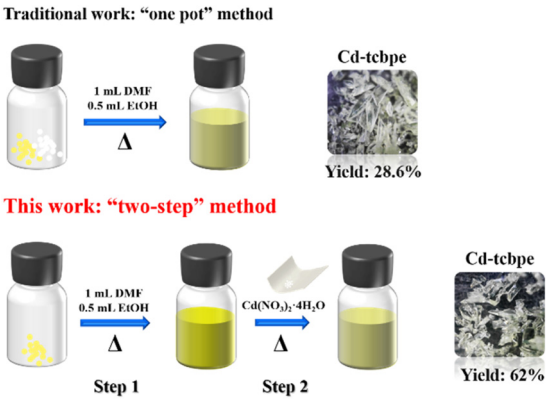

Scheme 1 Synthesis route of **Cd-tcbpe**.

3.2 Structural analysis of Cd-tcbpe

The coordination of $Cd(NO_3)_2\cdot 4H_2O$ and H_4tcbpe has been reported in the previous literature[33] at 80 °C. And in our attempt, the crystal obtained exhibits an identical structure (Tables S1 and S2†) and the detailed structure description of **Cd-tcbpe** is given in the ESI (Fig. S2†). But it is worth noting that there are two configurations of the deprotonated ligand $tcbpe^{4-}$ in the obtained MOF structure (Fig. 1a). Compared to the H_4tcbpe in the free conformation,[30] distortion occurs in the ligand after the formation of the framework structure (Fig. 1b). And two ligands with different coordination conformations exist in the structure at an angle of 70.525° (Fig. S3†). In addition, there are plenty of intermolecular interactions in the framework, such as C–H···π stacking interactions (Fig. S4 and Table S3†) and C–H···O hydrogen bond interactions (Fig. S5 and Table S4†). These intermolecular interactions can not only synergistically stabilize the skeleton, but also potentially facilitate the occurrence of intermolecular charge transfer, leading to emission and reducing the energy loss caused by non-radiative transition to a certain extent,[34] thus endowing **Cd-tcbpe** with superior luminescence efficiency.

3.3 Mechanochromic luminescence behavior of Cd-tcbpe

The obtained MOFs are pale yellow (Fig. 2a), with an absorption centred at 428 nm (Fig. 2b). In contrast, the absorption

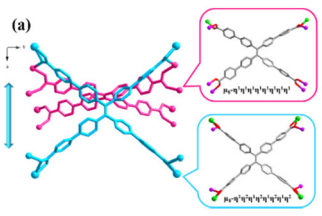

(b)	P1-P2 (°)	P1-P3 (°)	C=C double bond (Å)
H_4tcbpe[30]	50.20	12.26	1.341
Cd-tcbpe	53.12	43.97	1.350
	55.13	87.70	1.336

Fig. 1 (a) Connection modes of the H_4tcbpe ligand in **Cd-tcbpe**; (b) average dihedral angles and the distance of the C=C double bond of H_4tcbpe in the **Cd-tcbpe** conformation and in free conformation.[30]

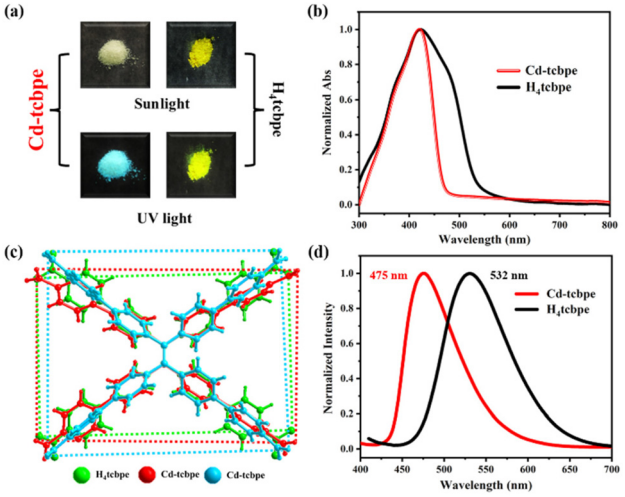

Fig. 2 (a) Emissive photographs of **Cd-tcbpe** and H_4tcbpe under a hand UV light of 365 nm; (b) UV-vis spectra of **Cd-tcbpe-B** and H_4tcbpe ligand; (c) comparison of tcbpe linkers in **Cd-tcbpe** (red, blue) and H_4tcbpe (green); (d) fluorescence emission spectra of **Cd-tcbpe** (λ_{ex} = 370 nm) and H_4tcbpe (λ_{ex} = 390 nm).

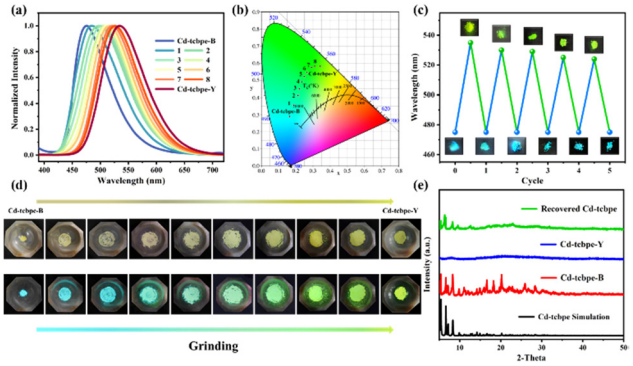

Fig. 3 (a) Fluorescence emission of **Cd-tcbpe** with the increase in grinding; (b) corresponding CIE coordinate changes; (c) recycling test of mechanochromic luminescence with grinding/restoring cycles; (d) representative color changes during the grinding process; (e) PXRD patterns of **Cd-tcbpe-B**, **Cd-tcbpe-Y**, recovered **Cd-tcbpe** and the simulated **Cd-tcbpe**.

spectrum of the bright yellow H_4tcbpe ligand has an additional shoulder peak at 501 nm (Fig. 2b). In the structure of the ligand H_4tcbpe, benzene rings connect through flexible σ bonds, and the change of the dihedral angle between the benzene ring and the plane will affect the color of the compounds. Therefore, the corresponding dihedral angles in the MOFs and ligand were measured respectively (as displayed in Fig. 1b); the free ligand has a higher degree of planarization compared to the ligand in MOFs, resulting in a more red-shifted absorption. In addition, the sizes of the rectangle formed by four oxygen atoms in the $tcbpe^{4-}$ linker are different, with 11.76 Å × 18.76 Å for H_4tcbpe (Fig. 2c, green) and 14.56 Å × 17.29 Å, 12.10 Å × 18.33 Å for **Cd-tcbpe** (Fig. 2c, red and blue). Thus, after being coordinated with the metal, the ligand undergoes an extension along a direction. This difference also leads to significant fluorescence differences[35] (Fig. 2d). **Cd-tcbpe** exhibits cyan colored emission at 475 nm with the coordinate (0.16, 0.29), whereas the H_4tcbpe ligand shows a yellow–green emission at 532 nm with the coordinate (0.33, 0.57) (Fig. S8b†). Moreover, DFT calculations were conducted to explain such differences.[35] The energy levels of the ligand and the protonated ligand in MOFs were calculated.[36] As displayed in Fig. S6,† the formation of the MOF increases the energy gap between the HOMO and LUMO of the ligand, leading to the blue shift of the emission peak. The fluorescence quantum yield of **Cd-tcbpe** is stable and reaches as high as 64.3%. In addition, **Cd-tcbpe** in crystalline state exhibits fluorescence emission at 475 nm at different excitation wavelengths (Fig. S7†).

Mechanochromic luminescence behavior represents one outstanding characteristic of TPE-based compounds. Hence, we investigated the fluorescence of crystalline **Cd-tcbpe** at different grinding levels. As shown in Fig. 3a, as the grinding frequency increases, the luminescence of **Cd-tcbpe** changes from cyan to yellow–green (Fig. 3b), and the corresponding emission spectra undergo a gradual red shift, with a maximum redshift of 60 nm. Meanwhile, the color of **Cd-tcbpe** also changes from pale yellow to bright yellow (Fig. 3d). Here, for convenience, we named the pre-grinding sample **Cd-tcbpe-B** and the maximum grinding sample **Cd-tcbpe-Y** based on the fluorescence color. It is worth mentioning that the fluorescence emission spectrum and CIE coordinate of **Cd-tcbpe-Y** are almost consistent with those of the ligand (Fig. S8b†), along with the UV-vis absorption spectrum (Fig. S8a†). Therefore, combined with Fig. 2c, it is believed that grinding leads to the compression of the ligand skeleton in MOFs, accompanied by the changes of color and luminescence. In contrast, the pure ligand could not change its own color and emission color, no matter how it was ground (Fig. S9†). So, the mechanochromic luminescence behavior of MOFs could be attributed to the coordinated framework structure, which could enable the existence of the unstable structure. Besides, as shown in Fig. S10a,† the photoluminescence quantum yield (PLQY) value of **Cd-tcbpe-Y** is 125.59%, higher than that of **Cd-tcbpe-B** (64.30%), and detailed descriptions of PLQY determination are shown in the ESI.† The fluorescence lifetime of **Cd-tcbpe-B** increased from 1.45 ns to 2.52 ns of **Cd-tcbpe-Y**, which means that the grinding process may lead to a slightly prolonged excitation state[34] (Fig. S10b†). The FT-IR spectrum of **Cd-tcbpe-Y** is almost identical to that of **Cd-tcbpe-B**, proving that the structure is maintained after grinding (Fig. S11†). Thermal analysis reveals smaller weight loss after grinding, indicating that the solvent molecules in the crystalline **Cd-tcbpe-B** are continuously lost during the grinding process (Fig. S12†). However, the PXRD pattern shows that after grinding, **Cd-tcbpe-Y** becomes amorphous (Fig. 3e), which is similar to the reported literature.[34]

The apparent color as well as fluorescence color of the ground MOFs could return to the initial color after treatment

with some solvents such as dichloromethane (DCM). Besides, it is found that the yellow powder could quickly change to the cyan one when immersed in the supernatant of the mixture after reaction. The use of such a solution is in accordance with the concept of green chemistry. The fluorescence spectrum and PXRD pattern of the solution treated **Cd-tcbpe-Y** are almost the same as those of the initial **Cd-tcbpe-B**, indicating that the reaction solution could help the recrystallization process and further restore cyan luminescence (Fig. 3e and S13†). Then the reversibility of such mechanochromic luminescence behavior was evaluated *via* alternately grinding and dispersing the ground powders into the reaction solution. As displayed in Fig. 3c, the ground powders could almost entirely recover to their initial color and fluorescence color after five-cycle experiments, revealing excellent reversibility. Besides, the FT-IR spectrum proves that the structure of **Cd-tcbpe** is maintained after cycling (Fig. S11,† blue). And the crystallinity of **Cd-tcbpe** recovered to 56.05% after cycling (the crystallinity of **Cd-tcbpe-B** is 87.65%) (Fig. 3e, green), which was calculated using Jade 6 software. Such good mechanochromic luminescence behaviors (*i.e.*, high sensitivity, excellent reversibility and obvious fluorescence difference before and after grinding) of **Cd-tcbpe** make it attractive for pressure sensing, anti-counterfeiting, *etc*.

To explore the further application of **Cd-tcbpe-B**, its paper-film based material was first prepared (see the details in the ESI†). The **Cd-tcbpe-B** powder was used to uniformly cover the surface of filter paper, which appears pale yellow in daylight, and shows cyan luminescence under UV light. By applying local pressure, the letters "ABCD" and the pattern of "heart" could be displayed and produce obviously different yellow fluorescence (Fig. 4a), thereby achieving patterning. Additionally, a flexible **Cd-tcbpe-B**@PMMA film was prepared *via* dispersing **Cd-tcbpe-B** into PMMA. Then the Chinese character "force" was written on such a film using a gel pen. It can be seen from Fig. 4b that the color and emission color of the Chinese character create a strong contrast with the background color. As mechanical scratches are one of the reasons that affect the service life of solid materials,[37] this sensitive material could also become one of the best choices to realize early detection of damage and also reduce the damage rate. We also tried to prepare a **Cd-tcbpe-B**@PDMS film with elasticity, but unfortunately **Cd-tcbpe** could not maintain its initial cyan color emission, displaying yellow-green fluorescence when being dispersed into PDMS, which leads to poor mechanochromic luminescence behavior (Fig. S14†). As a result, it is inferred that the polarity of the surroundings around **Cd-tcbpe** might affect the fluorescence of **Cd-tcbpe**. To confirm our conjecture, **Cd-tcbpe** was added to five different solvents with distinct polarities. It was found that on increasing the polarity of the solvent, the emission peaks of **Cd-tcbpe** gradually red shifted until it showed the maximum emission wavelength in water (Fig. S15†). Therefore, **Cd-tcbpe-B** exhibits yellow–green luminescence in the polymer PDMS with high polarity, while it displays cyan luminescence in the polymer PMMA with low polarity.

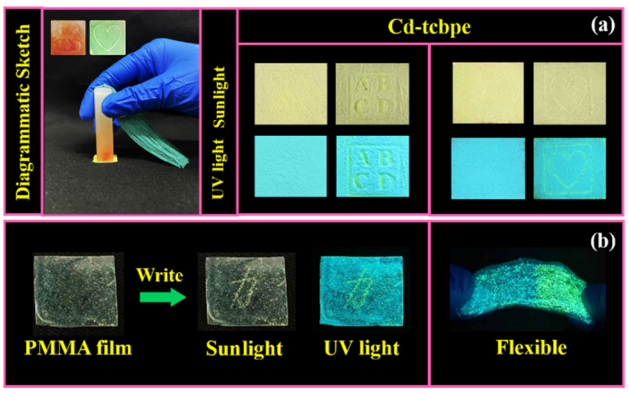

Fig. 4 (a) Seal photograph of "ABCD" and the pattern of a heart pressed on **Cd-tcbpe-B** under sunlight and UV light (365 nm); the picture on the left is a diagrammatic sketch, and in the upper left corner is a photograph of the seal with the letters "ABCD" and pattern of a heart; (b) images of **Cd-tcbpe-B**@PMMA films with the Chinese character "force" written using a gel pen.

3.4 White LED application of Cd-tcbpe-Y

Solid-state white LEDs[38] have opened up a promising path for green and environmentally friendly lighting due to their advantages of high efficiency, energy conservation, environmental friendliness, long durability and easy packaging.[39] They do not generate a large amount of energy waste compared to incandescent bulbs, nor do they pose a potential threat to the environment due to the leakage of mercury in fluorescence tubes.[40] Benefiting from the strong yellow–green emission of **Cd-tcbpe-Y** with high PLQY, its potential application for white LEDs was considered. According to the construction principle of white-emitting diodes, the MOF was first applied to a blue light LED. Unfortunately, no matter how much MOF was applied, when the LED was turned on, the **Cd-tcbpe-Y** based LED exhibited an emission with a CIE coordinate (0.25, 0.45), which is far away from the white light region. Due to a slight blue shift in the luminescence of **Cd-tcbpe-Y** compared to the yellow emission, the obtained **Cd-tcbpe-Y** based LED displayed green luminescence. For supplementing the luminescence in the range of 600 nm, a rose red LED was chosen instead. Notably, the emission of the rose red LED contains two parts: one emitting blue light centered at 450 nm and the other emitting pink light centered at 614 nm. The emission of blue light can stimulate the MOF to emit yellow–green fluorescence, due to the overlap between the luminescence and MOF absorption, while pink light could act as a supplement, rendering a white light emission. In considering this, the **Cd-tcbpe-Y** powder was integrated into a rose red light LED. As shown in Fig. 5a, when the additional amount is 10 mg, the **Cd-tcbpe-Y** based LED exhibits a white emission with a wide wavelength range and the CIE coordinate calculated was (0.30, 0.31) (Fig. 5b). Compared to the uncoated LED, the relative intensity of blue and pink light emission decreases when the **Cd-tcbpe-Y** based LED was lit, indicating the occurrence of an energy transfer

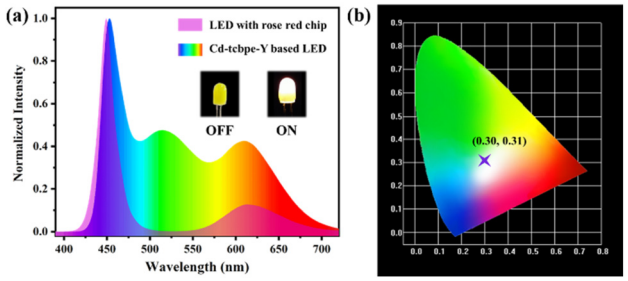

Fig. 5 (a) Fluorescence emission spectra of LED with a rose red chip and the **Cd-tcbpe-Y** based LED; (b) CIE coordinate for the **Cd-tcbpe-Y** based LED.

process. **Cd-tcbpe-Y** displayed a steady emission even on heating to 100 °C, which is beneficial for practical applications (Fig. S16†).

3.5 Hydrochromic luminescence behavior of Cd-tcbpe

It is worth noting that the dry **Cd-tcbpe-B** crystalline sample gradually changes from pale yellow to bright yellow accompanied by obvious fluorescence changes from cyan to yellow–green when exposed to air for 2 hours (Fig. S17 and S18,† yellow line), whereas it could still maintain its initial color when kept in a relatively dry environment. Thus, it is inferred that the water vapor in air might induce the color change. To confirm our supposition, **Cd-tcbpe-B** was soaked in ethanol solutions with different water contents for 5 min, and its solid-state fluorescence emission spectra were measured. As shown in Fig. 6, with increasing water content, the emission spectra peaks showed an apparent red shift from 475 to 517 nm, and the corresponding color changed from pale yellow to bright yellow, accompanied by an emission color change from cyan to yellow–green. In particular, when the water content exceeds 40%, the color change is very obvious. Nevertheless, we found that the color change rate during the grinding process was faster than that when it was placed in air, so it is speculated that water molecules have a little impact on the grinding process. As a result, on grinding **Cd-tcbpe-B** in a vacuum glovebox, the color and fluorescence changes still occurred (Fig. S18,† green line). Compared with the FT-IR spectra and PXRD pattern, before and after adding water, the crystallinity of the powder after hydrochromic luminescence decreased, but the structure did not show significant changes (Fig. S19†). As displayed in Fig. S19a,† the O–H stretching vibration peak around 3400 cm^{-1} ascribed to the OH functional groups red-shifted after addition of water, demonstrating the formation of hydrogen bonds in **Cd-tcbpe** after soaking in water. Moreover, the decrease of the O–H bending vibration peak (δ_{O-H}) at 1648 cm^{-1} also confirms this viewpoint. After solution treatment, the crystallinity and fluorescence could be restored. In addition, the obvious changes in color and fluorescence are still observed when placing the powder in an environment with low relative humidity (R.H. = 30%), revealing its potential to be applied in water vapor detection. Moreover, the hydrochromic luminescence mechanism is also comprehended that the exchange of H_2O molecules with a small size with internal DMF molecules caused the compression of the framework structure, leading to changes in the fluorescence spectra.

In addition to water, we found that some volatile acids or bases such as Et_3N, NH_3, CH_3COOH, CF_3COOH, and HCl all can induce color and fluorescence changes (Fig. 7a). Although the alkalinity of Et_3N is higher than that of NH_3, no obvious color changes occur. The color and fluorescence color changes rely on the exchange of the outside vapor and DMF molecules inside the MOF. NH_3, CH_3COOH, CF_3COOH, and HCl possess molecular sizes smaller than that of DMF; thus they could replace the DMF molecules in the structure and lead to a compression of the framework, leading a change of the emission color from cyan to yellow–green. In contrast, Et_3N with a size larger than that of DMF could not induce such conversion (Fig. S20†). Furthermore, different vapors cause different fluorescence displays (Fig. 7b). Such distinct fluorescence color differences detectable by the naked eye render **Cd-tcbpe** promising for acid/base vapor detection, and help quickly detect some vapors with molecular sizes larger than that of the DMF molecule. Besides, the thermochromic behavior of **Cd-tcbpe** has also been found (Fig. S21†). In addition, from the PXRD

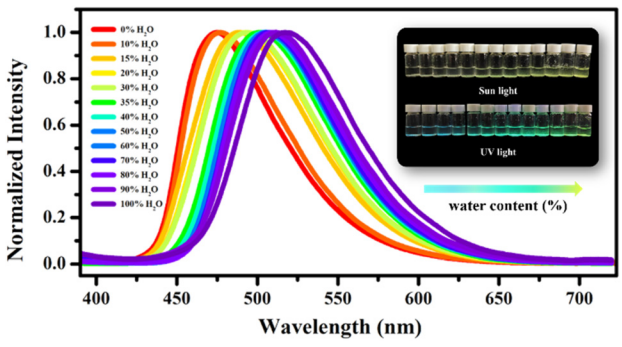

Fig. 6 Changes of fluorescence emission spectra of **Cd-tcbpe-B** with increasing water content (insert: the sunlight and UV light images of **Cd-tcbpe-B** in ethanol solutions with different water contents).

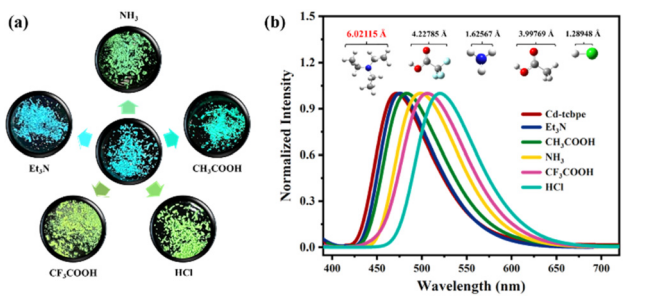

Fig. 7 Image (a) and fluorescence emission spectra (b) of **Cd-tcbpe-B** placed under five acid/base vapor environments with different sizes.

patterns (Fig. S22b†), it could be seen that **Cd-tcbpe-B** treated at lower temperatures could maintain its crystalline structure; however, once the temperature increased, **Cd-tcbpe-B** became amorphous; the IR spectra (Fig. S22a†) indicate that its structure has not changed after thermochromism. And the occurrence of thermochromic behavior could also be attributed to the compression of the framework due to the loss of solvent. Therefore, **Cd-tcbpe**, as a kind of multi-stimulus responsive MOF material, could be widely used in practical fields such as anti-counterfeiting, fluorescence sensing, vapor/temperature detection, *etc*.

4. Conclusion

In this work, we employed a "two-step" method, namely the ligand pre-heating method, to prepare a crystalline MOF material **Cd-tcbpe** with a three-dimensional porous network structure in a high yield. This type of crystalline material shows susceptible fluorescence color changes in response to mechanical forces, water, some small acid/base molecules and temperature. However, the above properties are not found in the ligand molecule. The emergence of this phenomenon is attributed to the configuration transformation of ligands in the framework structure. Therefore, the successful development of the multi-stimulus responsive properties of **Cd-tcbpe** has great potential in the field of anti-counterfeiting, information storage, white LEDs and fluorescence sensing.

Author contributions

Chen Wang: data curation, formal analysis, investigation, validation, and writing – original draft. Ting Zhang: data curation, investigation, and validation. Li-Xian Sun: funding acquisition. Yong-Heng Xing: investigation, supervision, validation, funding acquisition, and writing – review and editing. Feng-Ying Bai: supervision, validation, funding acquisition, and writing – review and editing.

Conflicts of interest

There are no conflicts to declare.

Acknowledgements

This work was supported by the Guangxi Bagui Scholar Foundation, the Science and Technology Development Project of Guilin (20210216-1, 20210102-4), the Postgraduate Education Reform Project of Liaoning Province (No. 394), and the grants of the National Natural Science Foundation of China (No. 21571091).

References

1 P. Yang, F. Zhu, Z. Zhang, Y. Cheng, Z. Wang and Y. Li, Stimuli-responsive polydopamine-based smart materials, *Chem. Soc. Rev.*, 2021, **50**, 8319–8343.
2 Q. Chen, X. Yu, Z. Pei, Y. Yang, Y. Wei and Y. Ji, Multi-stimuli responsive and multi-functional oligoaniline-modified vitrimers, *Chem. Sci.*, 2017, **8**, 724–733.
3 S. Zhang, S. Zhang, N. Yin, Z. Huang, W. Xu, K. Yue, X. Li and D. Li, Exploring Reversible Thermochromic Behavior in a Rare Ni(II)-MOF System, *ACS Appl. Mater. Interfaces*, 2021, **13**, 6430–6441.
4 E. Moulin, L. Faour, C. C. Carmona-Vargas and N. Giuseppone, From Molecular Machines to Stimuli-Responsive Materials, *Adv. Mater.*, 2020, **32**, 1906036.
5 M. Qu, L. Ma, J. Wang, Y. Zhang, Y. Zhao, Y. Zhou, X. Liu and J. He, Multifunctional Superwettable Material with Smart pH Responsiveness for Efficient and Controllable Oil/Water Separation and Emulsified Wastewater Purification, *ACS Appl. Mater. Interfaces*, 2019, **11**, 24668–24682.
6 L. Ding, S. Xuan, L. Pei, S. Wang, T. Hu, S. Zhang and X. Gong, Stress and Magnetic Field Bimode Detection Sensors Based on Flexible CI/CNTs–PDMS Sponges, *ACS Appl. Mater. Interfaces*, 2018, **10**, 30774–30784.
7 S. Chen, N. Zhang, B. Zhang, B. Zhang and J. Song, Multifunctional Self-Healing Ionogels from Supramolecular Assembly: Smart Conductive and Remarkable Lubricating Materials, *ACS Appl. Mater. Interfaces*, 2018, **10**, 44706–44715.
8 S.-J. Lim, B.-K. An, S. D. Jung, M.-A. Chung and S. Y. Park, Photoswitchable Organic Nanoparticles and a Polymer Film Employing Multifunctional Molecules with Enhanced Fluorescence Emission and Bistable Photochromism, *Angew. Chem., Int. Ed.*, 2004, **43**, 6346–6350.
9 Q. Yu, X. Su, T. Zhang, Y.-M. Zhang, M. Li, Y. Liu and S. X.-A. Zhang, Non-invasive fluorescence switch in polymer films based on spiropyran-photoacid modified TPE, *J. Mater. Chem. C*, 2018, **6**, 2113–2122.
10 X. Li, J. Yang and Y.-W. Yang, Recent advances of stimuli-responsive viologen-based nanocomposites, *Mater. Chem. Front.*, 2023, **7**, 1463–1481.
11 R. Hu, Y. Kang and B. Z. Tang, Recent advances in AIE polymers, *Polym. J.*, 2016, **48**, 359–370.
12 J. Luo, Z. Xie, J. W. Y. Lam, L. Cheng, H. Chen, C. Qiu, H. S. Kwok, X. Zhan, Y. Liu, D. Zhu and B. Z. Tang, Aggregation-induced emission of 1-methyl-1,2,3,4,5-pentaphenylsilole, *Chem. Commun.*, 2001, 1740–1741.
13 W. Huang, M. Bender, K. Seehafer, I. Wacker, R. R. Schröder and U. H. F. Bunz, A Tetraphenylethene-Based Polymer Array Discriminates Nitroarenes, *Macromolecules*, 2018, **51**, 1345–1350.
14 Z. Li, Y. Q. Dong, J. W. Y. Lam, J. Sun, A. Qin, M. Häußler, Y. P. Dong, H. H. Y. Sung, I. D. Williams, H. S. Kwok and B. Z. Tang, Functionalized Siloles: Versatile Synthesis,

Aggregation-Induced Emission, and Sensory and Device Applications, *Adv. Funct. Mater.*, 2009, **19**, 905–917.

15 Y. Hong, J. W. Y. Lam and B. Z. Tang, Aggregation-induced emission: phenomenon, mechanism and applications, *Chem. Commun.*, 2009, 4332–4353.

16 Y. Xiao, K. Zheng, N. Zhang, Y. Wang, J. Yan, D. Wang and X. Liu, Facile Synthesis of Tetraphenylethene (TPE)-Based Fluorophores Derived by π-Extended Systems: Opposite Mechanofluorochromism, Anti-Counterfeiting and Bioimaging, *Chem. – Eur. J.*, 2023, **29**, e202203772.

17 W. Huang, M. Bender, K. Seehafer, I. Wacker, R. R. Schröder and U. H. F. Bunz, Novel Functional TPE Polymers: Aggregation-Induced Emission, pH Response, and Solvatochromic Behavior, *Macromol. Rapid Commun.*, 2019, **40**, 1800774.

18 K. Li, Z. Li, D. Liu, M. Chen, S.-C. Wang, Y.-T. Chan and P. Wang, Tetraphenylethylene(TPE)-Containing Metal–Organic Nanobelt and Its Turn-on Fluorescence for Sulfide (S^{2-}), *Inorg. Chem.*, 2020, **59**, 6640–6645.

19 Y. Lu, C. Liu, C. Mei, J. Sun, J. Lee, Q. Wu, M. A. Hubbe and M.-C. Li, Recent advances in metal organic framework and cellulose nanomaterial composites, *Coord. Chem. Rev.*, 2022, **461**, 214496.

20 H. Daglar, H. C. Gulbalkan, G. Avci, G. O. Aksu, O. F. Altundal, C. Altintas, I. Erucar and S. Keskin, Effect of Metal–Organic Framework (MOF) Database Selection on the Assessment of Gas Storage and Separation Potentials of MOFs, *Angew. Chem., Int. Ed.*, 2021, **60**, 7828–7837.

21 H. Xiang, Y. Shao, A. Ameen, H. Chen, W. Yang, P. Gorgojo, F. R. Siperstein, X. Fan and Q. Pan, Adsorptive separation of C2H6/C2H4 on metal-organic frameworks (MOFs) with pillared-layer structures, *Sep. Purif. Technol.*, 2020, **242**, 116819.

22 X.-M. Tian, S.-L. Yao, C.-Q. Qiu, T.-F. Zheng, Y.-Q. Chen, H. Huang, J.-L. Chen, S.-J. Liu and H.-R. Wen, Turn-On Luminescent Sensor toward Fe^{3+}, Cr^{3+}, and Al^{3+} Based on a Co(II) Metal–Organic Framework with Open Functional Sites, *Inorg. Chem.*, 2020, **59**, 2803–2810.

23 A. E. Thorarinsdottir and T. D. Harris, Metal–Organic Framework Magnets, *Chem. Rev.*, 2020, **120**, 8716–8789.

24 M. Rivera-Torrente, L. D. B. Mandemaker, M. Filez, G. Delen, B. Seoane, F. Meirer and B. M. Weckhuysen, Spectroscopy, microscopy, diffraction and scattering of archetypal MOFs: formation, metal sites in catalysis and thin films, *Chem. Soc. Rev.*, 2020, **49**, 6694–6732.

25 W. Fan, X. Wang, B. Xu, Y. Wang, D. Liu, M. Zhang, Y. Shang, F. Dai, L. Zhang and D. Sun, Amino-functionalized MOFs with high physicochemical stability for efficient gas storage/separation, dye adsorption and catalytic performance, *J. Mater. Chem. A*, 2018, **6**, 24486–24495.

26 J.-X. Wang, J. Yin, O. Shekhah, O. M. Bakr, M. Eddaoudi and O. F. Mohammed, Energy Transfer in Metal–Organic Frameworks for Fluorescence Sensing, *ACS Appl. Mater. Interfaces*, 2022, **14**, 9970–9986.

27 S.-H. Huang, C.-H. Lin, W.-C. Wu and S.-L. Wang, Network Topology of a Hybrid Organic Zinc Phosphate with Bimodal Porosity and Hydrogen Adsorption, *Angew. Chem., Int. Ed.*, 2009, **48**, 6124–6127.

28 J. Liu, Y.-Z. Fan, K. Zhang, L. Zhang and C.-Y. Su, Engineering Porphyrin Metal–Organic Framework Composites as Multifunctional Platforms for CO_2 Adsorption and Activation, *J. Am. Chem. Soc.*, 2020, **142**, 14548–14556.

29 A. Bavykina, N. Kolobov, I. S. Khan, J. A. Bau, A. Ramirez and J. Gascon, Metal–Organic Frameworks in Heterogeneous Catalysis: Recent Progress, New Trends, and Future Perspectives, *Chem. Rev.*, 2020, **120**, 8468–8535.

30 Z. Wei, Z.-Y. Gu, R. K. Arvapally, Y.-P. Chen, R. N. McDougald, Jr., J. F. Ivy, A. A. Yakovenko, D. Feng, M. A. Omary and H.-C. Zhou, Rigidifying Fluorescent Linkers by Metal–Organic Framework Formation for Fluorescence Blue Shift and Quantum Yield Enhancement, *J. Am. Chem. Soc.*, 2014, **136**, 8269–8276.

31 X.-D. Xu, Y. Liang, A. Mensah, J.-F. Li, L. Zhou, L.-Z. Chen and F.-M. Wang, Synthesis, Structures and Fluorescence Properties of Two Novel Cadmium MOFs Based on a Tetraphenylethene(TPE)-Core Ligand, *ChemistrySelect*, 2019, **4**, 12380–12385.

32 C. Wang, R. Huo, F. Xu, Y.-H. Xing and F.-Y. Bai, Multiple stimulus responsive Co-AIE framework materials with reversible solvatochromic and thermochromic behaviors: molecular design, synthesis and characterization, *J. Mater. Chem. C*, 2022, **10**, 17723–17733.

33 F.-M. Wang, L. Zhou, W. P. Lustig, Z. Hu, J.-F. Li, B.-X. Hu, L.-Z. Chen and J. Li, Highly Luminescent Metal–Organic Frameworks Based on an Aggregation-Induced Emission Ligand as Chemical Sensors for Nitroaromatic Compounds, *Cryst. Growth Des.*, 2018, **18**, 5166–5173.

34 X. Ma, X. Xu, F. Duan, W. Huang, Q. Chen and D. Wu, High-Efficiency Wideband Excitable Mechanoluminescence from a Yellow MOF Phosphor as White LED and Multicolor Thin Films, *Adv. Opt. Mater.*, 2022, **10**, 2101461.

35 Q. Zhang, J. Su, D. Feng, Z. Wei, X. Zou and H.-C. Zhou, Piezofluorochromic Metal–Organic Framework: A Microscissor Lift, *J. Am. Chem. Soc.*, 2015, **137**, 10064–10067.

36 M. J. Frisch, G. W. Trucks, H. B. Schlegel, G. E. Scuseria, M. A. Robb, J. R. Cheeseman, G. Scalmani, V. Barone, B. Mennucci, G. A. Petersson, H. Nakatsuji, M. Caricato, X. Li, H. P. Hratchian, A. F. Izmaylov, J. Bloino, G. Zheng, J. L. Sonnenberg, M. Hada, M. Ehara, K. Toyota, R. Fukuda, J. Hasegawa, M. Ishida, T. Nakajima, Y. Honda, O. Kitao, H. Nakai, T. Vreven, J. A. Montgomery, Jr., J. E. Peralta, F. Ogliaro, M. Bearpark, J. J. Heyd, E. Brothers, K. N. Kudin, V. N. Staroverov, R. Kobayashi, J. Normand, K. Raghavachari, A. Rendell, J. C. Burant, S. S. Iyengar, J. Tomasi, M. Cossi, N. Rega, J. M. Millam, M. Klene, J. E. Knox, J. B. Cross, V. Bakken, C. Adamo, J. Jaramillo, R. Gomperts, R. E. Stratmann, O. Yazyev, A. J. Austin, R. Cammi, C. Pomelli, J. W. Ochterski, R. L. Martin, K. Morokuma, V. G. Zakrzewski, G. A. Voth, P. Salvador,

J. J. Dannenberg, S. Dapprich, A. D. Daniels, O. Farkas, J. B. Foresman, J. V. Ortiz, J. Cioslowski and D. J. Fox, Gaussian, Inc., Wallingford CT, 2009.

37 W. Yin, Z. Yang, S. Zhang, Y. Yang, L. Zhao, Z. Li, B. Zhang, S. Zhang, B. Han and H. Ma, A positively charged aggregation-induced emission (AIE) luminogen as an ultra-sensitive mechanochromic luminescent material: design, synthesis and versatile applications, *Mater. Chem. Front.*, 2021, **5**, 2849–2859.

38 Y. Tang, H. Wu, W. Cao, Y. Cui and G. Qian, Luminescent Metal–Organic Frameworks for White LEDs, *Adv. Opt. Mater.*, 2021, **9**, 2001817.

39 S. Ye, F. Xiao, Y. X. Pan, Y. Y. Ma and Q. Y. Zhang, Phosphors in phosphor-converted white light-emitting diodes: Recent advances in materials, techniques and properties, *Mater. Sci. Eng., R*, 2010, **71**, 1–34.

40 N. Armaroli and V. Balzani, Towards an electricity-powered world, *Energy Environ. Sci.*, 2011, **4**, 3193–3222.